DOI 10.1007/s11182-024-03150-z
Russian Physics Journal, Vol. 67, No. 5, May, 2024

EVOLUTION OF SHOCK WAVES IN Fe-Ni SAMPLES WITH DIFFERENT STRUCTURE

A. V. Korchuganov, D. S. Kryzhevich, A. S. Grigoriev, O. A. Berezikov, and K. P. Zolnikov

UDC 533.6.011.72

A molecular dynamics study of the shock wave evolution in single-crystalline and nanocrystalline $Fe_{95}Ni_{05}$ *samples with a gradient grained structure is carried out at different shock loading rates. An analysis of the compressive stress distribution in loaded samples is performed. The spatiotemporal intervals of the plastic and elastic material responses and the features of the shock wave evolution during their propagation are revealed. It is shown that a shock wave at high compressive stresses splits into elastic and plastic components. Compressive stresses in the region of a plastic wave are higher than in the region of an elastic wave. The time interval for reaching a stationary regime of shock wave propagation and the features of the maximum stress decrease depend both on the shock compression rate and on the material internal structure. At higher loading rates in the sample with a gradient grained structure, the stress in the shock wave decreases faster than in a single crystal.*

Keywords: shock wave, compressive stress, single crystal, gradient nanograined alloy, molecular dynamics.

INTRODUCTION

Nanocrystalline materials with a gradient grained structure have unique physical and mechanical properties combining high strength and ductility. They can be effectively used in many practical applications under extreme conditions, for example, under ion or radiation exposure, cyclic mechanical and shock loadings. All of these harsh service conditions lead to a generation of various wave disturbances in materials, shock waves among them. The gradient grained structure can have a significant influence on the characteristics of wave generation and propagation due to the high density of interfaces and its variation from the free surface of a material to its bulk.

One of the most effective ways to study the behavior of materials at the microscopic level under shock loading is the method of molecular dynamics (MD) simulations [1–5]. This method makes it possible to accurately calculate the characteristics of a shock wave and identify the structural transformations [6–12], the phase transitions [13–17] at the wave propagation front, and the spallation features [18–23], when the shock wave reaches the rear surface of the sample. The MD method was successfully used to study the response of various structural materials, in particular nanocrystalline materials, to shock loading [24–28].

The study of nanocrystalline, amorphous, polymeric, biological, and energetic materials shows that the parameters of disturbances and processes initiated by shock loading strongly depend on the structure of the loaded material [24, 29–31]. The influence of microstructure (grain boundaries) and crystallographic orientations on the behavior of a nanocrystalline hcp Ti sample with a columnar grain shape under shock loading was studied by Wang et al. [24]. An MD simulation revealed that the nucleation and development of shock-induced plasticity and phase transitions in such materials have a pronounced anisotropy. The simulations of shock loading from 40 to 100 GPa of

Institute of Strength Physics and Materials Science of the Siberian Branch of the Russian Academy of Sciences, Tomsk, Russia, e-mail: avkor@ispms.ru; kryzhev@ispms.ru; grigoriev@ispms.ru; berezikov07@ispms.ru; kost@ispms.ru. Original article submitted February 29, 2024.

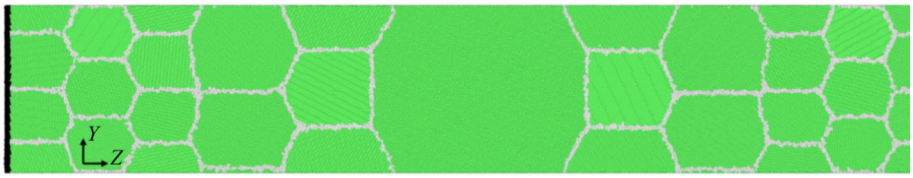

Fig. 1. Section of the gradient nanograined sample in the *YZ* plane. The impactor is highlighted in black, the atoms of grains and grain boundaries are marked in green and gray, respectively.

single- and nanocrystalline tantalum revealed a number of differences in their response, which can be explained by the interactions between the neighboring grains [25]. Thus, a joint elastic deformation of the neighboring grains in the normal direction to shock loading can reduce both the shear stress and the deformation. The stress changes caused by grain interactions can activate and deactivate the plasticity mechanisms depending on the shock pressure. In turn, this makes it possible to control the dislocation density during sample loading. Thus, the intergranular interactions under shock loading play an important role in the material deformation behavior. Sichani et al. [26] studied the deformation of nanocrystalline copper depending on the grain size and orientation under shock loading using the MD method. The shock loading at the rates from 1.0 to 3.4 km/s was applied to nanocrystalline samples with the grain sizes from 6 to 26 nm. It was found out that the grain size and orientation and the loading rate have a significant effect on the fraction of a bcc structure forming behind the shock wave front. The relation between the plasticity and the bcc-hcp structural phase transformation in an iron single crystal under shock and ramp compression was studied in the framework of the MD method [6]. In both cases, the simulated iron sample yielded through twinning. In this case, the onset of a bcc-hcp structural phase transformation significantly depended on the history of plasticity due to the hardening effect, which can inhibit the nucleation of the hcp phase. A non-equilibrium MD simulation of shock compression along the [001] direction in the Ta single crystal with pre-existing defects was carried out by Tramontina [7]. The strain rate was reported to have a significant effect on the flow stress and dislocation density behind the shock wave front. The calculation results are in an excellent agreement with the experimental data on strength and recovered microstructure, which "*goes from dislocations to a mixture of dislocations and twins*" to the subsequent predominance of the twinning process with the increasing shock pressure [7].

The above results show that the shock loading schemes and parameters have a strong influence on the material deformation behavior. In turn, the structure of the material largely determines the parameters of shock waves generated by shock loading. It is advisable to conduct a detailed study of the influence of the structure on the shock wave parameters based on a comparison of the structural responses of single-crystalline and nanocrystalline samples. Such a comparison can be most effectively implemented within the MD framework. In this work, we study the features of a shock-wave evolution in the single-crystal and nanocrystalline $Fe_{95}Ni_{05}$ samples with a gradient grained structure under shock compression.

SIMULATION METHODOLOGY AND ANALYSIS ALGORITHMS

The study of the features of the nonlinear response in the $Fe_{95}Ni_{05}$ alloy with a single-crystalline and nanocrystalline gradient grained structure under shock loading was carried out on the basis of an MD simulation. The calculations were performed in the LAMMPS software package [32]. An interatomic interaction in the Fe-Ni system was described by a many-body potential developed in the approximation of the embedded atom method [33]. The Common Neighbor Analysis algorithm [34] was used to identify the structural changes in the loaded samples.

The gradient grained structure of the sample was constructed by the Voronoi–Laguerre method. All grains in the sample had a common crystallographic direction coinciding with the *Z* texture axis with indices [123] (Fig. 1). In the direction of the *Z* axis, starting from the free surface, the layers were successively arranged, in each of which the grains had the following sizes in nm: 10, 10, 10, 15, 15, 30, 15, 15, and then 10 nm. The periodic boundary conditions were

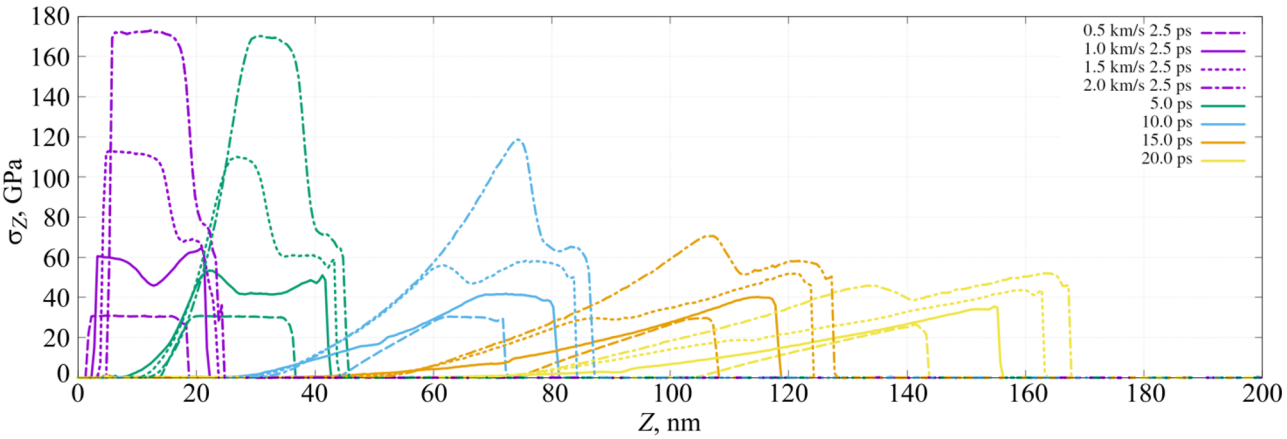

Fig. 2. Distributions of compressive stresses in the *Z* direction in the single crystal at different time instants for different loading rates.

used along the *X* and *Y* directions, and free surfaces were specified in the *Z* direction. The *X*, *Y*, *Z* axes of the single crystal were oriented along the crystallographic directions $[1\bar{2}1]$, $[41\bar{2}]$ and [123], respectively. The samples had the shape of parallelepipeds with the dimensions of 30×30×500 nm. The initial temperature of the samples was set to 300°K.

To set the shock loading, a 5 Å thick layer was selected on the left free surface of the samples, simulating an impactor. It was displaced for 3 ps as an absolutely rigid body, and then released from the loading. The displacement velocity of the impactor varied in different calculations from 0.5 to 2.0 km/s.

SIMULATION RESULTS AND DISCUSSION

It is advisable to begin the study of the shock wave evolution in the simulated alloy using the samples with an ideal crystal lattice. This will make it possible to determine not only the conditions of their nucleation and the features of propagation under the chosen loading scheme, but also to further understand the mechanisms of their interaction with the extended interfaces in the case of a gradient nanograined sample. The structural transformations in the shock wave region and the evolution of its characteristics can be simulated based on the calculation of compressive stresses. The results of calculations of the stress component distribution in the shock wave propagation direction for the impactor velocities in the interval from 0.5 to 2.0 km/s are presented in Fig. 2. The figure clearly shows that not only the compressive stress magnitude, but also the shock wave profile significantly depend on the loading rate. This is most clearly manifested at the time points of 2.5 and 5.0 ps after the start of loading. The compressive stress distribution profile in the shock wave region changes its shape as the impactor velocity increases: at 0.5 km/s it is quite flat and at higher velocities the stresses increase non-uniformly along the wave profile due to its splitting into elastic and plastic components. A plastic wave is characterized by significantly higher compressive stresses. The elastic-plastic splitting of the shock wave is confirmed by the data on the behavior dynamics of the materials under impact, shock, stress and high-strain rate deformations [35], and by high-quality X-ray diffraction data on the subnanosecond dynamics of laser-shocked polycrystalline iron [36].

By the time interval of 10–15 ps, the compressive stresses in the shock wave region decrease quite strongly and the profiles of the front part of the waves flatten (Fig. 2). The difference in the maximum stresses for different impactor velocities decreases due to a more intense generation of structural defects, which enhances the shock wave energy dissipation. In 15–20 ps, the shock wave energy becomes insufficient to generate any structural defects. Then the shock waves propagate through the sample at a constant velocity, virtually without changing the shape of their profile.

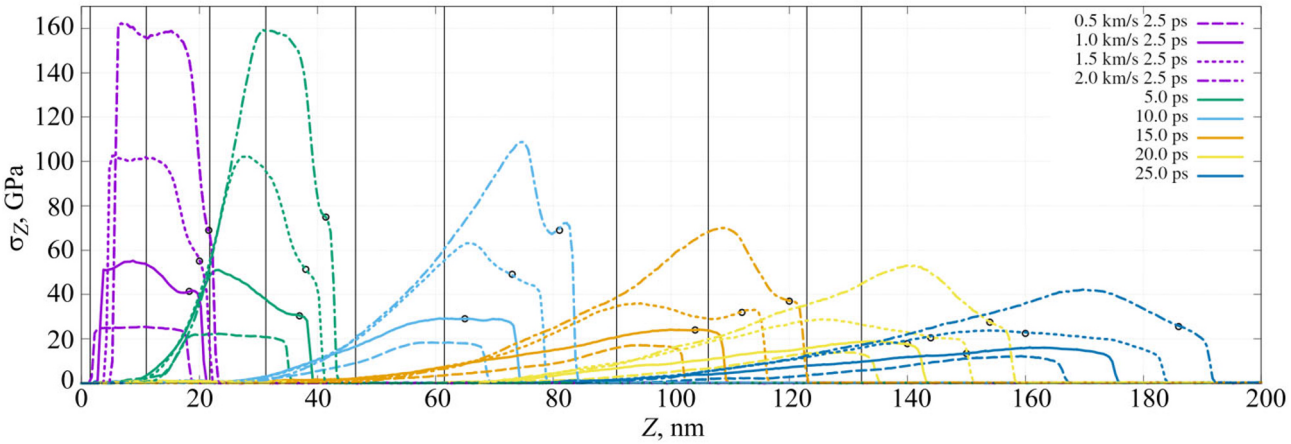

Fig. 3. Distributions of compressive stresses in the *Z* direction in the gradient nanograined sample at different time instants for different loading rates. Circles indicate the plasticity wave front. Vertical lines show the layer boundaries with different grain sizes before loading.

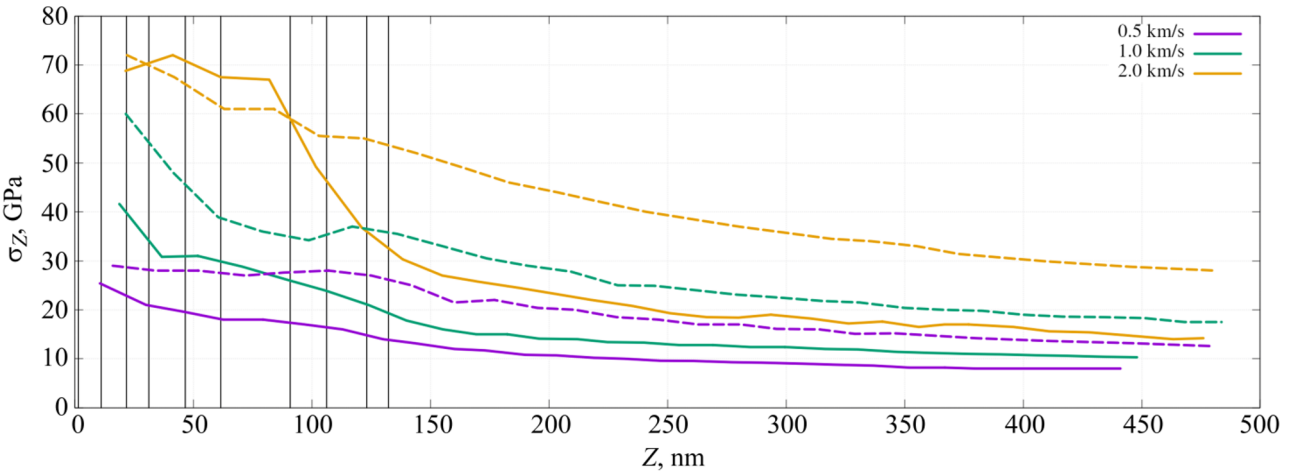

Fig. 4. Compressive stresses in the *Z* direction in an elastic wave versus the coordinates of its front for the single crystal (dashed lines) and gradient nanograined samples (solid lines). Vertical lines show the boundaries of layers with different grain sizes before loading.

The stress profiles of shock waves during their propagation in a nanocrystalline material with a gradient grained structure are presented in Fig. 3. Similarly to the case of a single-crystal sample, the wave splits into elastic and plastic components as the impactor velocity increases.

Depending on the loading rate, the maximum compressive stresses in the shock wave region quickly decrease over time to the values of 10–25 GPa and then virtually cease to change. However, the rate of decrease of the maximum stresses and the time interval for them to reach a stationary value strongly depend on the impactor velocity. For example, the maximum value of compressive stress at an impactor velocity of 0.5 km/s decreases from 25 to 10 GPa in 45 ps, and at a velocity of 2.0 km/s it decreases from 160 to 17 GPa in 60 ps. The stresses in an elastic wave in the sample with the gradient grained structure are lower, and the rate of their decrease is much higher than in the single crystal under the same loading conditions (Fig. 4). Moreover, the stresses are reduced more effectively at a higher impactor velocity in the gradient nanograined sample compared to the single-crystal sample. It should be noted that

both for the single-crystalline and gradient nanograined samples, the width of the region with an increased value of compressive stresses increases with time (Figs. 2 and 3). This is due to a lower rate of the material structure accommodation process compared to the velocity of shock wave propagation.

CONCLUSIONS

A molecular dynamics simulation of the single-crystal and gradient nanograined $Fe_{95}Ni_{05}$ samples has shown that the parameters of shock waves and the features of their propagation in this material can be effectively studied based on an analysis of the spatiotemporal evolution of compressive stresses. As part of this analysis, the spatiotemporal intervals of the plastic and elastic material responses during the shock wave propagation were identified. These intervals were determined by the changes in the shape of the compressive stress profile. It was revealed that a shock wave at high compressive stresses splits into elastic and plastic components. The compressive stresses in the region of the plastic wave are higher than in the elastic wave. It has been shown that the maximum compressive stresses and stresses in the elastic part of the wave during shock compression of the sample decrease quite quickly and reach a stationary value. The time interval for reaching a stationary regime of shock wave propagation and the features of the maximum stress decrease depend both on the shock compression rate and on the material internal structure. Moreover, the stresses in the shock wave decrease quicker at higher impactor velocities in the gradient nanograined sample compared to the single-crystal sample.

COMPLIANCE WITH ETHICAL STANDARDS

Author contributions

A.V.K.: conceptualization, writing of initial draft; D.S.K. and A.S.G.: development of the simulation approaches and performing the computations; O.A.B.: visualization of simulation results; K.P.Z.: verification and analysis of the simulation results. All authors discussed the results and contributed to the final manuscript. All authors have read and agreed to the published version of the manuscript.

Conflicts of interest

The authors declare that they have no known competing financial interests or personal relationships that could have appeared to influence the work reported in this paper.

Funding

The study of the single-crystalline sample was carried out according to the Government Assignment for the ISPMS SB RAS (Project No. FWRW-2021-0002). The study of the gradient nanograined sample was financially supported by the Russian Science Foundation (Project No. 20-79-10406), https://rscf.ru/project/20-79-10406/.

Financial interests

The authors have no relevant financial or non-financial interests to disclose.

Institutional review board statement

Applicable.

REFERENCES

1. K. Binder, J. Horbach, W. Kob, *et al*., J. Phys. Condens. Matter, **16**, S429–S453 (2004); https://doi.org/10.1088/0953-8984/16/5/006.
2. D. C. Rapaport, The Art of Molecular Dynamics Simulation (Cambridge University Press, 2004); https://doi.org/10.1017/cbo9780511816581.
3. S. G. Psakhie, S. Y. Korostelev, S. I. Negreskul, *et al.*, Phys. Status Solidi, **176**, K41–K44 (1993); https://doi.org/10.1002/pssb.2221760227.
4. S. G. Psakhie, K. P. Zolnikov, and D. Yu. Saraev, J. Mater. Sci. Technol., **14**, 475–477 (1998)
5. S. G. Psakhie, K. P. Zolnikov, and D. Yu. Saraev, J. Mater. Sci. Technol., **14**, 72–74 (1998)
6. N. Amadou, T. De Resseguier, A. Dragon, and E. Brambrink, Phys. Rev. B, **98**, 024104 (2018); https://doi.org/10.1103/PhysRevB.98.024104.
7. D. Tramontina, P. Erhart, T. Germann, *et al.*, High Energy Density Phys., **10**, 9–15 (2014); https://doi.org/10.1016/j.hedp.2013.10.007.
8. G. Mogni, A. Higginbotham, K. Gaál-Nagy, *et al.*, Phys. Rev. B, **89**, 064104 (2014); https://doi.org/10.1103/PhysRevB.89.064104.
9. A. Neogi, and N. Mitra, Comput. Mater. Sci., **135**, 141–151 (2017); https://doi.org/10.1016/j.commatsci.2017.04.009.
10. P. Wen, G. Tao, C. Pang, *et al.*, Comput. Mater. Sci., **124**, 304–310 (2016); https://doi.org/10.1016/j.commatsci.2016.08.010.
11. N. Gunkelmann, Y. Rosandi, C.J. Ruestes, *et al.*, Comput. Mater. Sci., **119**, 27–32 (2016); https://doi.org/10.1016/j.commatsci.2016.03.035.
12. B. Cao, E. M. Bringa, and M. A. Meyers, Metall. Mater. Trans. A Phys. Metall. Mater. Sci. **38 A**, 2681–2688 (2007); https://doi.org/10.1007/s11661-007-9248-9.
13. N. Gunkelmann, E. M. Bringa, D. R. Tramontina, *et al.*, Phys. Rev. B, **89**, 140102 (2014); https://doi.org/10.1103/PhysRevB.89.140102.
14. Y. Huang, Y. Xiong, P. Li, *et al.*, Int. J. Plast., **114**, 215–226 (2019); https://doi.org/10.1016/j.ijplas.2018.11.004.
15. G. Li, Y. Wang, K. Wang, *et al.*, J. Appl. Phys., **126**, 075902 (2019); https://doi.org/10.1063/1.5097621.
16. K. Wang, W. Zhu, S. Xiao, et al., Int. J. Plast., **71**, 218–236 (2015); https://doi.org/10.1016/j.ijplas.2015.01.002.
17. H. Zong, X. Ding, T. Lookman, and J. Sun, Acta Mater., **115**, 1–9 (2016); https://doi.org/10.1016/j.actamat.2016.05.037.
18. E. N. Hahn, T. C. Germann, R. Ravelo, *et al.*, Acta Mater., **126**, 313–328 (2017); https://doi.org/10.1016/j.actamat.2016.12.033.
19. X. Tian, J. Cui, K. Ma, and M. Xiang, Int. J. Heat Mass Transf., **158**, 120013 (2020); https://doi.org/10.1016/j.ijheatmasstransfer.2020.120013.
20. G. Agarwal, and A. M. Dongare, Comput. Mater. Sci., **145**, 68–79 (2018); https://doi.org/10.1016/j.commatsci.2017.12.032.
21. W. Li, E.N. Hahn, X. Yao, *et al.*, Acta Mater., **167**, 51–70 (2019); https://doi.org/10.1016/j.actamat.2018.12.035.
22. L. He, F. Wang, X. Zeng, *et al.*, Mech. Mater., **143**, 103343 (2020); https://doi.org/10.1016/j.mechmat.2020.103343.
23. S. Galitskiy, D. S. Ivanov, and A. M. Dongare, J. Appl. Phys., **124**, (2018); https://doi.org/10.1063/1.5051618.

24. L. Wang, B. Li, X. L. Deng, *et al.*, Phys. Rev. B, **99**, 174103 (2019); https://doi.org/10.1103/PhysRevB.99.174103.
25. P. G. Heighway, D. McGonegle, N. Park, *et al.*, Phys. Rev. Mater., **3**, 083602 (2019); https://doi.org/10.1103/PhysRevMaterials.3.083602.
26. M. M. Sichani and D. E. Spearot, Comput. Mater. Sci., **108**, 226–232 (2015); https://doi.org/10.1016/j.commatsci.2015.07.021.
27. S. C. Hu, J. W. Huang, Z. D. Feng, *et al.*, J. Appl. Phys., **129**, (2021); https://doi.org/10.1063/5.0033153.
28. H. T. Luu, R. J. Ravelo, M. Rudolph, *et al.*, Phys. Rev. B, **102**, 020102 (2020); https://doi.org/10.1103/PhysRevB.102.020102.
29. K. V. Reddy, C. Deng, and S. Pal, Acta Mater., **164**, 347–361 (2019); https://doi.org/10.1016/j.actamat.2018.10.062.
30. M. A. N. Dewapriya and R. E. Miller, J. Appl. Mech. Trans. ASME, **88**, 101005 (2021); https://doi.org/10.1115/1.4051238.
31. P. Das, P. Zhao, D. Perera, *et al.*, J. Appl. Phys., **130**, 085901 (2021); https://doi.org/10.1063/5.0056560.
32. S. Plimpton, J. Comput. Phys., **117**, 1–19 (1995); https://doi.org/10.1006/jcph.1995.1039.
33. X.W. Zhou, M.E. Foster, and R.B. Sills, J. Comput. Chem., **39**, 2420–2431 (2018); https://doi.org/10.1002/jcc.25573.
34. J. D. Honeycutt, and H. C. Andersen, J. Phys. Chem., **91**, 4950–4963 (1987); https://doi.org/10.1021/j100303a014.
35. M. A. Meyers, Dynamic behavior of materials. dynamic behavior of materials (Wiley, 2007); https://doi.org/10.1002/9780470172278.
36. H. Hwang, E. Galtier, H. Cynn, *et al.*, Sci. Adv., **6**, eaaz5132 (2020); https://doi.org/10.1126/sciadv.aaz5132.